

# An isotopic effect in $\phi$ photoproduction at a few GeV

A. Titov<sup>a,b\*</sup>, T.-S.H. Lee<sup>c†</sup> and H. Toki<sup>a‡</sup>,

<sup>a</sup> *Research Center for Nuclear Physics, Osaka University, Osaka 567-0047, Japan*

<sup>b</sup> *Bogoliubov Laboratory of Theoretical Physics, JINR, Dubna 141980, Russia*

<sup>c</sup> *Physics Division, Argonne National Laboratory, Argonne, IL 60439, USA*

## Abstract

A distinct isotopic effect in  $\phi$  photoproduction at  $\sqrt{s} \sim 2 - 5$  GeV region is identified by examining the production amplitudes due to Pomeron-exchange and meson-exchange mechanisms. This effect is mainly caused by the  $\pi$ - $\eta$  interference constrained by SU(3) symmetry and the isotopic structure of the  $\gamma NN$  coupling in the direct  $\phi$ -radiation amplitude. It can be tested experimentally by measuring differences in the polarization observables between the  $\gamma p \rightarrow \phi p$  and  $\gamma n \rightarrow \phi n$  reactions.

PACS number(s): 13.88.+e, 24.70.+s, 25.20.Lj, 13.60.Le

Typeset using REVTeX

---

\*E-mail address : [atitov@thsun1.jinr.ru](mailto:atitov@thsun1.jinr.ru)

†E-mail address : [lee@anph09.phy.anl.gov](mailto:lee@anph09.phy.anl.gov)

‡E-mail address : [toki@rcnp.osaka-u.ac.jp](mailto:toki@rcnp.osaka-u.ac.jp)

**Introduction.** Traditionally, the  $\gamma p \rightarrow \phi p$  reaction is considered as a tool to study the Pomeron exchange dynamics, implying that (i) the vector meson dominance model (VDM) [1,2] is valid, and (ii) other hadronic mechanisms are suppressed by OZI rule. The Pomeron-exchange mechanism is depicted in Fig.1a. Together with an examination of the conventional Pomeron trajectory with an intercept  $\alpha(0) \sim 1.08$  [2–6], it has been suggested that this reaction can be used to probe more exotic processes associated with additional trajectories including the glueball trajectory [7].

In order to learn about the Pomeron structure and possible manifestation of more exotic dynamics, such as the hidden strangeness in proton (cf. [8,9] for references), one should first fix the “non-strange” background determined by the conventional mechanisms. Namely, we need to evaluate as accurately as possible the leading amplitudes due to the pseudo-scalar ( $\pi, \eta$ )-exchange (PSE) and the direct  $\phi$ -radiation from the nucleon legs. They are illustrated in Fig.1b and Fig.1c respectively. The  $\eta$ -exchange and direct  $\phi$ -radiation mechanisms are of current interest. In particular, the coupling constant  $g_{\eta NN}$  is not well established and it is subject to further investigations. Similarly, our understanding of  $\phi NN$  coupling is still limited. Its OZI-violation value has been evaluated, for example in Ref. [10], by considering the finite  $\phi\pi\rho$  couplings and the interaction of the  $\phi$ -meson with the kaon cloud of the nucleon.

A step towards an understanding of the structure of the “non-strange” background in  $\phi$  photoproduction is taken in a recent paper [11]. The focus of Ref. [11] is to explore the possibility of determining the  $\phi NN$  and  $\eta NN$  coupling constants using the  $\gamma p \rightarrow \phi p$  reaction. Except the  $\pi NN$  coupling constant, all parameters associated with Pomeron-exchange,  $\eta$  exchange, and direct  $\phi$ -radiation amplitudes are adjusted to fit the data. In this paper we take a different approach. We calculate the ( $\pi, \eta$ )-exchange, and the direct  $\phi$ -radiation amplitudes using the parameters *predetermined* in previous works constrained by SU(3) symmetry. This will allow us to pin down the parameters associated with an additional Pomeron trajectory that will be introduced later.

In Ref. [12] we give a detailed analysis of  $\phi$  photoproduction amplitudes in a few GeV region and predict all spin density matrix elements that are needed to evaluate various observables associated with the  $K^+ K^-$  angular distributions from the decay of the produced  $\phi$  meson. In the present Letter we emphasis an interesting isotopic effect caused by the  $\pi$ - $\eta$  interference(Fig.1b) and the difference between the photon-proton and photon-neutron vertices in the direct  $\phi$ -radiation mechanism(Fig.1c). Experimental tests of our predictions will help pin down the ”non-strange” background of  $\phi$  photoproduction.

We define the kinematical variables for the  $\gamma + N \rightarrow \phi + N$  reaction using standard notations. The four-momenta of the incoming photon, outgoing  $\phi$ , initial nucleon, and final nucleon are denoted as  $k, q, p,$  and  $p'$ , respectively. The usual Mandelstam variables are then defined as  $t = (p - p')^2 = (q - k)^2$  and  $s \equiv W^2 = (p + k)^2$ . The masses of the nucleon, pion, and  $\phi$  meson are  $M_N, M_\pi,$  and  $M_\phi$  respectively. We use the conventions of Bjorken&Drell to define the  $\gamma$  matrices and Dirac spinors.

**Pomeron exchange amplitudes.** A microscopic model for vector-meson photo- and electro-production at high energies based on the Pomeron-photon analogy has been proposed by Donnachie and Landshoff [3] (DL-model). It is assumed that the incoming photon first converts into a quark-antiquark pair, which then exchanges a Pomeron with the nucleon before recombining into an outgoing  $\phi$  meson, as depicted in Fig. 2. It can be shown

that the data at high energies can be described by a Pomeron trajectory with an intercept  $\alpha(0) \sim 1.08$ . This trajectory will be called the  $P_1$  trajectory in this paper. Within Regge theory, it is easy to see that the  $P_1$  trajectory can only be identified with objects with spin  $J > 0$ . It was suggested [7] that a different Pomeron trajectory, as inspired by the glueball ( $J^\pi = 0^+, M_{\text{gb}}^2 \simeq 3 \text{ GeV}^2$ ) predicted by Lattice QCD calculations and a QCD-based Dual Landau-Ginsburg model [13], could dominate the cross section at low energies by having a negative intercept  $\alpha(0)$ . This Pomeron trajectory, called  $P_2$ , will be also considered in this work.

The DL-model was examined in Ref. [2] by using an Euclidean QCD model of mesons to evaluate exactly the quark-loop integration in Fig.2. It was shown that the interpretation of the Pomeron as gluonic object is consistent with the data up to very large  $Q^2$  and  $W$ . For the  $Q^2 = 0$  and  $W < 5 \text{ GeV}$  region considered in this work, the exact loop integration, as done in Ref. [2], can be approximated by the factorized form employed by Donnachie and Landshoff. We therefore follow Donnachie and Landshoff and use this simplified version of the model to define the Pomeron-exchange amplitudes. We will not consider two-gluon-exchange models of Pomeron as proposed in Refs. [4,5,14].

Within the DL-model, the invariant amplitude can be written as

$$T_{fi}^{P_n} = M_0^{P_n} \varepsilon_{\phi\mu}^* \mathcal{M}^{P_n\mu\nu} \varepsilon_{\gamma\nu}, \quad \mathcal{M}^{P_n\mu\nu} = \mathcal{F}_\alpha^{P_n} \Gamma^{P_n\alpha,\mu\nu}, \quad (1)$$

where  $\varepsilon_{\gamma\nu}$  and  $\varepsilon_{\phi\mu}$  are respectively the polarization vectors of the photon and  $\phi$  meson,  $\mathcal{F}_\alpha^{P_n}$  describes the Pomeron-nucleon vertex, and  $\Gamma^{P_n\alpha,\mu\nu}$  is associated with the Pomeron-vector-meson coupling which is related to the  $\gamma \rightarrow q\bar{q}$  vertex  $\Gamma_\nu$  and the  $q\bar{q} \rightarrow \phi$  vertex  $V_\mu$ , as shown in Fig. 2. We follow the DL-model and assume that the  $P_1$ -nucleon coupling is photon-like. For the  $P_2$ -nucleon vertex, we assume a scalar coupling. Accordingly, we have

$$\mathcal{F}_\alpha^{P_n} = \bar{u}(p') g_\alpha^{P_n} u(p), \quad g_\alpha^{P_1} = \gamma_\alpha, \quad g_\alpha^{P_2} = 1, \quad (2)$$

where  $u(p)$  is the nucleon spinor with momentum  $p$ . By using the factorization approximation of Donnachie and Landshoff, an explicit evaluation [9] of the Dirac algebra associated with the quark-loop shown in Fig.2 leads to the following form of the Pomeron-vector meson coupling in Eq.(1)

$$\Gamma^{P_1\alpha,\mu\nu} = g^{\alpha\nu} k^\mu - k^\alpha g^{\mu\nu}, \quad \Gamma^{P_2\mu\nu} = (k^\mu q^\nu - k \cdot q g^{\mu\nu})/M_\phi, \quad (3)$$

where the transversality conditions  $\mathcal{M}^{P_{1,2}\mu\nu} \cdot q_\mu = \mathcal{M}^{P_{1,2}\mu\nu} \cdot k_\nu = 0$  are fulfilled. The strength factors  $M_0^{P_{1,2}}$  in Eq.(1) take the conventional form of Regge parameterization

$$M_0^{P_i} = C_i F(t) F_i(s, t) e^{-i\frac{\pi}{2}\alpha_i(t)} \left( \frac{s - s_i}{s_0} \right)^{\alpha_i(t)}, \quad (4)$$

where the trajectories are taken to be

$$\alpha_1(t) = \alpha_1(0) + \alpha'_1 t = 1.08 + 0.25 t, \quad \alpha_2(t) = -0.75 + 0.25 t, \quad s_0 = \alpha'^{-1}. \quad (5)$$

As discussed above,  $\alpha_1(t)$  is chosen to fit the data at large  $s$  and  $\alpha_2(t)$  is inspired by the ( $J^\pi = 0^+, M_{\text{gb}}^2 \sim 3 \text{ GeV}^2$ ) glueball, predicted by Lattice QCD calculations and a QCD-based

Dual Landau-Ginsburg model [13]. We follow Ref. [6] to define the overall form factor in Eq.(4) as  $F(t) = F_\phi(t) \cdot F_N(t)$  [6] with

$$F_N(t) = (M_N^2 - 2.8t) / ((4M_N^2 - t)(1 - (t/0.7))^2), \quad F_\phi(t) = \exp[B(t - t_{\max})]. \quad (6)$$

The correcting functions  $F_{1,2}(s, t)$  for Eq.(4) are

$$F_i^{-2} = \Gamma_{\mu\nu}^{P_i\alpha} \Gamma_{\mu'\nu'}^{P_i\alpha'} \text{Tr} \{g_\alpha^{P_i}(\not{p}' + M_N)g_{\alpha'}^{P_i}(\not{p}' + M_N)\} (g^{\mu\mu'} - q^\mu q^{\mu'}/M_\phi^2) g^{\nu\nu'}/4M_N^2. \quad (7)$$

The strength factor  $C_1$  in Eq.(4) is chosen to reproduce  $d\sigma/dt|_{\theta=0}$  at large  $s$ , where the cross section is entirely due to  $P_1$  trajectory. The strength factor  $C_2$  is chosen to reproduce  $d\sigma/dt|_{\theta=0}$  at low energies where all mechanisms shown in Fig.1 are important. The slope  $B$  is chosen to reproduce the available data of angular distributions,  $d\sigma/dt$ . Note that the phase of the Pomeron exchange amplitudes is fixed and controlled by the exponential factors in (4). At  $t = 0$ ,  $P_1$  amplitude is almost purely imaginary and negative, while the  $P_2$  amplitude is complex.

**Pseudoscalar exchange amplitudes.** We calculate the  $(\pi, \eta)$ -exchange by using the following effective Lagrangians

$$\mathcal{L}_{\phi\gamma\varphi} = \frac{e}{M_\phi} g_{\phi\gamma\varphi} \epsilon^{\mu\nu\alpha\beta} \partial_\mu \phi_\nu \partial_\alpha A_\beta \varphi, \quad (8)$$

$$\mathcal{L}_{PS} = \frac{g_{\pi^0 NN}}{2M_N} \bar{N} \gamma_\mu \gamma_5 \tau_3 N \partial^\mu \pi^0 + \frac{g_{\eta NN}}{2M_N} \bar{N} \gamma_\mu \gamma_5 N \partial^\mu \eta, \quad (9)$$

where  $\varphi = \pi^0, \eta$ , and  $A_\beta$  is the photon field. For the  $\pi NN$  coupling, we use the standard value  $g_{\pi NN} = (4\pi \cdot 14)^{1/2}$ . The status of the  $\eta NN$  coupling is not so clear. The value of  $g_{\eta NN}^2/4\pi$  reported in the literatures varies from 0 to about 7. The largest value comes from fits to NN scattering data, using one boson exchange potential models [15]. But many other studies [16–19] favor a smaller value,  $g_{\eta NN}^2/4\pi \sim 0.3 - 1.0$ . In our calculation we accept the SU(3) symmetry prediction [20] based on the most recent value of  $F/D = 0.575$  [21]. This leads to  $g_{\eta NN} = (0.99 \cdot 4\pi)^{1/2}$  which is close to its ‘‘overall’’ averaged value. Later, we will discuss how our prediction of polarization observables can be used to pin down the value of  $g_{\eta NN}$ .

The magnitude of the coupling constant  $g_{\phi\gamma\varphi}$  in Eq.(8) can be estimated through the decay widths [22] of  $\phi \rightarrow \gamma\pi$  and  $\phi \rightarrow \gamma\eta$ . We obtain  $|g_{\phi\gamma\pi}| = 0.14$  and  $|g_{\phi\gamma\eta}| = 0.707$ . Consistent with our choice of  $\eta NN$  coupling constant discussed above, we also employ the SU(3) symmetry to determine their signs. We find that their signs are the same but are opposite to the sign of  $g_{\omega\gamma\pi}$ , which is found to be positive in the pion photoproduction [23,24]. Since  $g_{\eta pp}$  and  $g_{\pi^0 pp}$  (here we include the sign due to the matrix element of the isospin factor  $\tau_3$ ) have the same sign, we expect a *constructive* interference between  $\pi$ - and  $\eta$ -exchange amplitudes in the  $\gamma p \rightarrow \phi p$  reaction. The situation changes in  $\gamma n \rightarrow \phi n$  reaction. In this case the isospin property determines that  $g_{\pi^0 nn} (= -g_{\pi^0 pp})$  is of opposite sign of  $g_{\eta nn} (= g_{\eta pp})$  and hence the corresponding interference becomes *destructive*.

The vertices in Fig.1b must be dressed by form factors. We choose the standard form  $F_{\varphi NN}(t) = (\Lambda_\varphi^2 - M_\varphi^2)/(\Lambda_\varphi^2 - t)$  and  $F_{\phi\gamma\varphi}(t) = (\Lambda_{\phi\gamma\varphi}^2 - M_\varphi^2)/(\Lambda_{\phi\gamma\varphi}^2 - t)$ . Here we assume that the range of the  $\pi$ -exchange is identical to that determined by Friman and Soyeur [25] in their study of  $\rho$  and  $\omega$  photoproduction. This leads us to choose  $\Lambda_\pi = 0.7$  GeV and

$\Lambda_{\phi\gamma\pi}^\pi = 0.77$  GeV. There is no reliable source to fix the cutoff parameters of the  $\eta$ -exchange amplitude. For definiteness, we set  $\Lambda_\eta = 1$  GeV and  $\Lambda_{\phi\gamma\eta} = 0.9$  GeV which are the values for the  $\sigma$ -exchange determined by Friman and Soyeur [25] in their fit to the  $\rho$  photoproduction. These choices of cutoff parameters represent the main uncertainty of our predictions. Nevertheless, they are comparable to the values used in the literature and are sufficient for the present investigation. We find that our main conclusion concerning the isotopic effect is not changed unless very hard form factors ( $\Lambda_\alpha >$  about 1.5 GeV) are used. The hard form factors are in general not favored in reproducing the total cross sections at high energies.

**Direct  $\phi$  – radiation amplitude.** We evaluate this amplitude(Fig.1c) by using the following interaction Lagrangians

$$\mathcal{L}_{\gamma NN} = -e \left( \bar{N} \gamma_\mu \frac{1 + \tau_3}{2} N A^\mu - \frac{\kappa_N}{2M_N} \bar{N} \sigma^{\mu\nu} N \partial_\nu A_\mu \right), \quad (10)$$

$$\mathcal{L}_{\phi NN} = -g_{\phi NN} \left( \bar{N} \gamma_\mu N \phi^\mu - \frac{\kappa_\phi}{2M_N} \bar{N} \sigma^{\mu\nu} N \partial_\nu \phi_\mu \right), \quad (11)$$

with  $\kappa_{p(n)} = 1.79(-1.91)$ . The resulting direct and crossed amplitudes in Fig.1c are real and their signs are controlled by the constants  $g_{\phi NN}$  and  $\kappa_\phi$ . Here we choose  $g_{\phi NN} = -0.24$  and  $\kappa_\phi = 0.2$ , which are obtained from an estimate [10] of the OZI-violation contributions due to  $\phi\pi\rho$  couplings and the interaction of  $\phi$  with the kaon cloud of the nucleon. The calculation of Ref. [10] is also constrained by SU(3) symmetry, consistent with our evaluation of the  $(\pi, \eta)$ -exchange amplitudes discussed above.

The  $\phi NN$  vertices in Fig.1c may be dressed by form factors. Namely, the direct and crossed terms must be dressed by  $F_s^\phi$  and  $F_u^\phi$  respectively. A possible form is [11,26]  $F_a^\phi(a) = \Lambda_\phi^4 / (\Lambda_\phi^4 + (a - M_N^2)^2)$ ,  $a = s, u$ . But this results in strong violation of gauge invariance with respect to the photon and  $\phi$  meson fields. One can use the gauge invariant prescription of [27], where a universal form factor  $F^\phi(s, u) = \frac{1}{2}(F_s^\phi(s) + F_u^\phi(u))$  is used to regularize both  $\phi NN$  vertices. But our predictions would then have an additional uncertainty [27] depending on the cutoff parameter  $\Lambda_\phi$ . To avoid this problem we use the prescription of [28] and simply set  $F_s^\phi = F_u^\phi = 1$ . Our prediction of the contribution from the direct  $\phi$ -radiation(Fig.1c) may therefore be considered as an upper limit.

**Results.** With the  $(\pi, \eta)$ -exchange and direct  $\phi$ -radiation amplitudes defined above, our first task is to determine the parameters of Pomeron-exchange amplitudes. The parameters  $s_i$  and  $C_i$  of Eq.(4) are not independent in the fit to the data. For example, a smaller value of  $s_2$  will lead to a larger  $C_2$  in the fit. For simplicity we set  $s_2 = 0$ . To account for the threshold behavior of the  $P_1$  amplitude, we set  $s_1 = \sqrt{M_N + M_\phi}$ . We then find that the  $d\sigma/dt(\theta = 0)$  data of  $\gamma p \rightarrow \phi p$  reaction can be reproduced with  $\xi = C_2/C_1 = -0.55$  and  $C_1 = 2.34$ . Our result is the thick solid curve in the left panel of Fig.3. The slope  $B = 1.7$  GeV $^{-2}$  of the form factor Eq.(6) is needed to reproduce the angular distribution, as shown in the right panel of Fig.3. Here we also display the relative importance between different amplitudes. We note that the  $P_1$  contribution drops sharply as energy approaches the production threshold. On the other hand, the  $P_2$  contribution increases very quickly as energy decreases. This striking difference in energy-dependence between  $P_1$  and  $P_2$  is due to the different signs of their intercepts:  $\alpha_1(0) = 1.08$  and  $\alpha_2(0) = -0.75$ (see Eq.(5)). By comparing the  $\pi$ -curve and  $(\pi, \eta)$ -curve in Fig.3, we see that the  $\pi$  and  $\eta$  amplitudes interfere constructively. This

is exactly what we expected in the discussion given above. The direct  $\phi$ -radiation clearly dominates the cross sections at large angles.

The fits to the  $\gamma p \rightarrow \phi p$  data completely fix the model and we can now apply the model to predict the  $\phi$  photoproduction on neutron. Our results for  $\gamma n \rightarrow \phi n$  are shown in Fig.4. For comparison, we also display the corresponding  $\gamma p \rightarrow \phi p$  results. Here we observe that  $\pi$ - and  $\eta$ -exchange interfere destructively (comparing the  $\pi$ -curve and  $(\pi, \eta)$ -curve). The direct  $\phi$ -radiation contribution (dash-dotted curves) is drastically different from that in Fig.3. This is due to the large difference between the  $\gamma pp$  and  $\gamma nn$  vertices. However, the change in the cross sections due to this isotopic effect is very small except at large scattering angles (comparing the top two curves in Fig.4) where the cross sections are very small. Experimental verification of this prediction is very difficult.

We now point out that the isotopic effect discussed above can be verified by examining polarization observables. As an example, we show in Fig.5 our prediction of the  $\phi$  decay asymmetry [29]

$$\Sigma_\phi = \frac{\sigma_{\parallel} - \sigma_{\perp}}{\sigma_{\parallel} + \sigma_{\perp}}, \quad (12)$$

where  $\sigma_{\parallel}(\sigma_{\perp})$  are the cross sections induced by photons polarized in the direction parallel (perpendicular) to the  $\gamma - \phi$  plane. These two cross sections refer to measurements of the symmetric  $K^+K^-$  pairs produced in the  $\phi$  decay. Our prediction of  $\Sigma_\phi$  at  $E_\gamma = 2$  GeV are shown in Fig.5. We find that the predicted isotopic effect at forward angles is largely due to the  $\pi - \eta$  interference. This can be understood by comparing the  $(\pi, \eta)$ -curve and  $\phi NN$ -curve in the right panels of Figs. 3 and 4. Consequently, the predicted energy-dependence at  $\theta = 0$  shown in the left panel of Fig.6 can be used to explore the relatively undetermined  $\eta NN$  coupling constant. To facilitate such a study, we show the dependence of  $\Sigma_\phi(\theta = 0)$  on  $g_{\eta NN}$  in the right panel of Fig.6. In this calculation, the strength  $C_2$  of the  $P_2$  Pomeron is adjusted to maintain the same fit to the  $\gamma p \rightarrow \phi p$  data as  $g_{\eta NN}$  is varied in the calculation. At large angles, the cross sections are dominated by the direct  $\phi$ -radiation amplitude. Hence a measurement of  $\Sigma_\phi$  at large angles can be used to study the  $\phi NN$  coupling. However, such a measurement may be very difficult because the cross sections become very small at large angles.

In summary, we have developed a model to describe the  $\phi$  photoproduction at low energies,  $\sqrt{s} \sim 2 - 5$  GeV. In addition to the traditional Pomeron trajectory with an intercept of  $\alpha_1(0) = 1.08$ , the model contains a second Pomeron trajectory with a negative intercept  $\alpha_2(0) = -0.75$  inspired by the ( $J^\pi = 0^+$ ,  $M_{\text{gb}}^2 \sim 3$  GeV) glueball predicted by Lattice QCD calculations and a QCD-based Dual Landau-Ginsburg model [13]. The model also includes the contributions from  $(\pi, \eta)$ -exchange and direct  $\phi$ -radiation from the nucleon. We have found a strong isotopic effect in the predicted  $\phi$  decay asymmetry (Figs.5, 6), indicating the possibility of using the  $\phi$  photoproduction polarization observables to explore the  $\eta NN$  and  $\phi NN$  couplings. Experiments for measuring such observables at LEPS of SPring-8 (Japan) and TJNAF (USA) are highly desirable.

**Acknowledgments.** We gratefully acknowledge useful discussions with M. Fujiwara, T. Hotta, T. Morii, T. Nakano, Y. Oh, E. Oset and D. Roy. A.I.T. appreciates support of the COE professorship program and the warm hospitality of the Research Center for Nuclear

Physics of Osaka University. This work is also partially supported by the U.S. Department of Energy, Nuclear Physics Division, under Contract NO. W-31-109-ENG-38.

## REFERENCES

- [1] A. Donnachie and P. V. Landshoff, Nucl. Phys. **B267** (1986) 690.
- [2] M. A. Pichowsky and T.-S. H. Lee, Phys. Rev. D **56** (1997) 1644.
- [3] A. Donnachie and P. V. Landshoff, Phys. Lett. B **185** (1987) 403.
- [4] P. V. Landshoff and O. Nachtmann, Z. Phys. C **35** (1987) 405.
- [5] A. Donnachie and P. V. Landshoff, Phys. Lett. B **296** (1992) 227.
- [6] J.-M. Laget and R. Mendez-Galain, Nucl. Phys. **A581** (1995) 397.
- [7] T. Nakano and H. Toki, in Proc. of Intern. Workshop on Exciting Physics with New Accelerator Facilities, SPring-8, Hyogo, 1997, World Scientific Publishing Co. Pte. Ltd.,1998, p.48.
- [8] J. Ellis, M. Karliner, D.E. Kharzeev, M.G. Sapozhnikov, Phys. Lett. B **353** (1995) 319.
- [9] A.I. Titov, Y. Oh, S.N. Yang, Morii, Phys. Rev. C **58** (1998) 2429.
- [10] U.-G. Meissner, V. Mull, J. Speth, J.W. Van Orden, Phys. Lett. B **408** (1997) 381.
- [11] R.A. Williams, Phys. Rev. C **57** (1998) 223.
- [12] A.I. Titov, T.-S. H. Lee, H. Toki and O. Streltsova, *in preparation*.
- [13] H. Suganuma, S. Sasaki and H. Toki, Nucl. Phys. **B435** (1995) 207.
- [14] J. R. Cudell, Nucl. Phys. **B336** (1990) 1.
- [15] R. Brockmann and R. Machleidt, Phys. Rev. C **42** (1989) 189.
- [16] W. Grein and P. Kroll, Nucl. Phys. **A338** (1980) 332.
- [17] J. Piekarewicz, Phys. Rev. C **48** (1993) 1555.
- [18] T. Hatsuda, Nucl. Phys. **B329** (1990) 376.
- [19] B. Krusche et al., Phys. Rev. Lett. **74** (1995) 3736.
- [20] J.J. De Swart, Rev. Mod. Phys. **35** (1963) 916.
- [21] F.E. Close and R.D. Roberts, Phys. Lett. B **316** (1993) 165.
- [22] Review of Particle Physics **C3** (1998) 1.
- [23] M. Gari and H. Hyuga, Nucl. Phys. **A264** (1976) 409.
- [24] T. Sato and T.-S. H. Lee, Phys. Rev. C **54** (1996) 2660.
- [25] B. Friman and M. Soyeur, Nucl. Phys. **A600** (1996) 477.
- [26] C. Piarce and B.K. Jennings, Nucl. Phys. **A528** (1991) 655.
- [27] H. Haberzettl, Phys. Rev. C **56** (1997) 2041; nucl-th/9804051.
- [28] K. Ohta, Phys. Rev. C **40** (1989) 1335.
- [29] K. Schilling, P. Seybothg, G. Wolf Nucl. Phys. **B15** (1970) 397.
- [30] H. Ballam et al., Phys. Rev. C **7** (1974) 3150.
- [31] H. Besh et al., Nucl. Phys. **B70** (1973) 257.
- [32] J. Behrend et al., Nucl. Phys. **B144** (1978) 22.



FIGURES

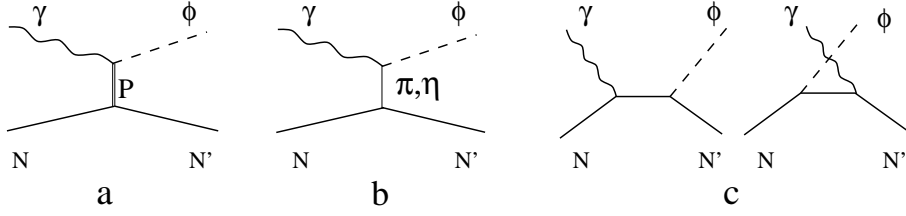


FIG. 1. Diagrammatic representation of  $\phi$  production mechanisms: (a) Pomeron-exchange, (b)  $(\pi, \eta)$ -exchange, and (c) direct  $\phi$ -radiation.

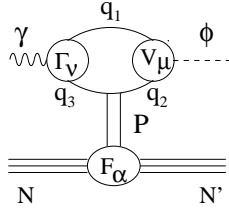


FIG. 2. Diagrammatic representation of the Donnachie-Landshoff model of Pomeron exchange

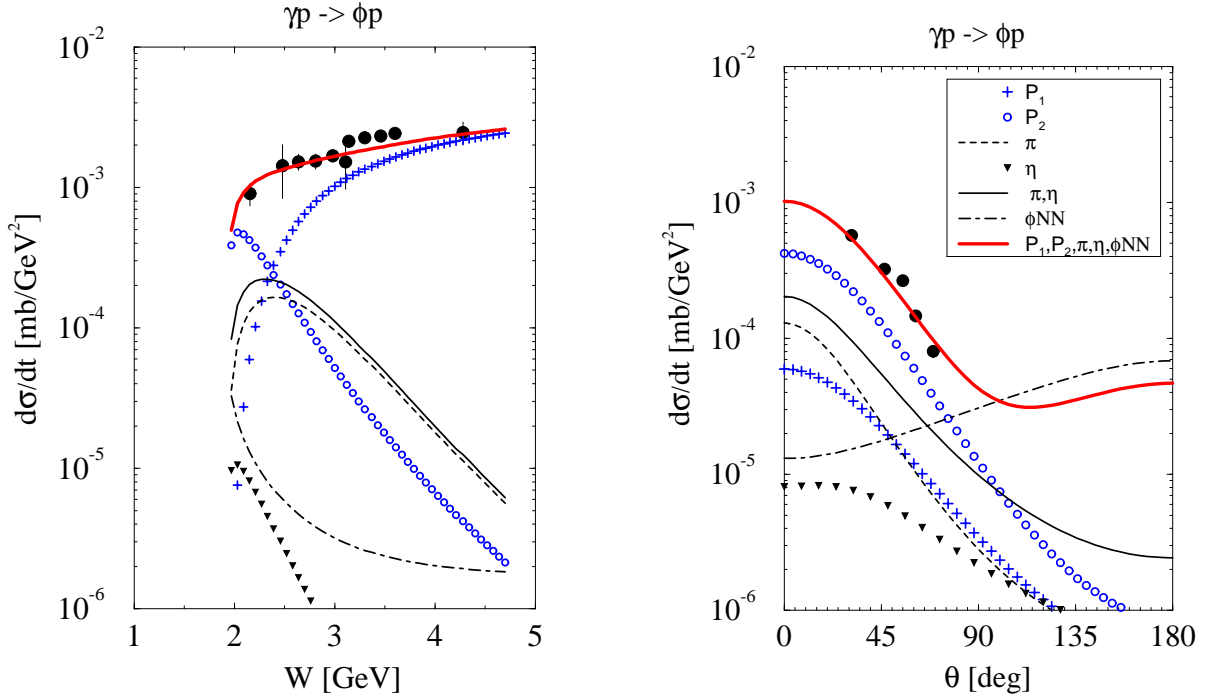


FIG. 3. Right panel: differential cross section for the  $\gamma p \rightarrow p\phi$  reaction at  $t = t_{\max}$  ( $\theta = 0$ ) as a function of the total energy  $W = \sqrt{s}$ . Data are taken from [30–32] Right panel: differential cross section at  $E_\gamma = 2$  GeV ( $W = 2.15$  GeV). Data are taken from [30].

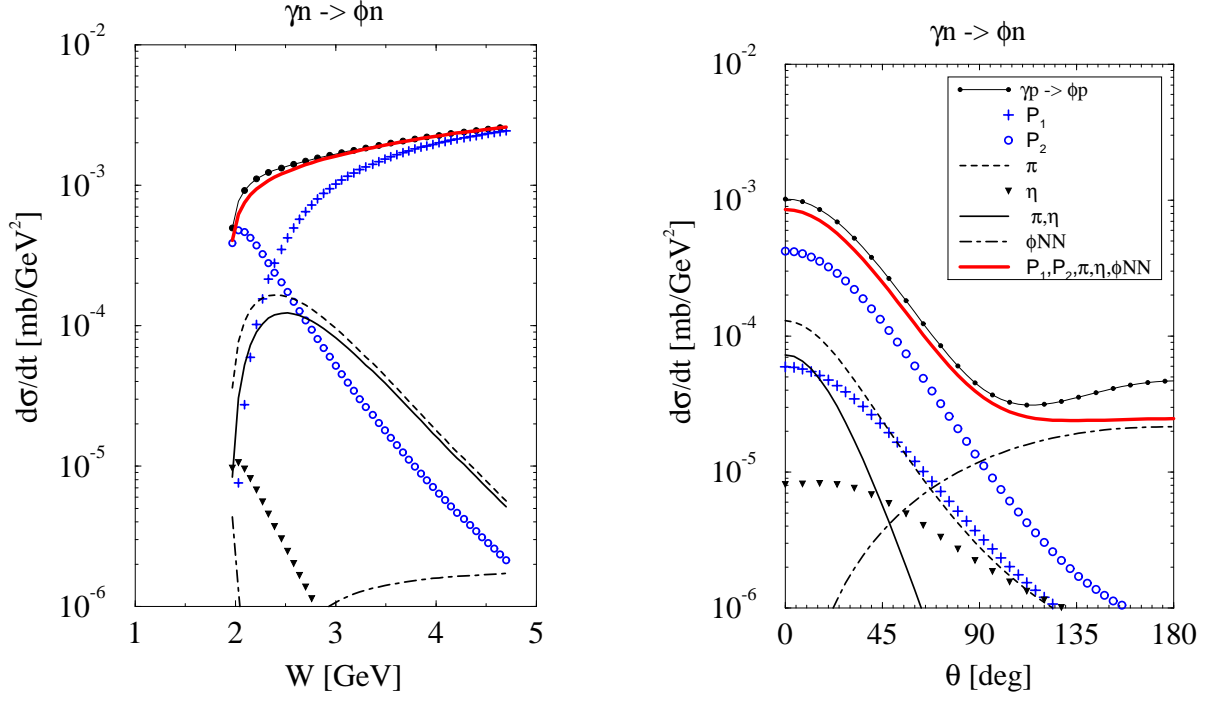


FIG. 4. Same as Fig.3 except for the  $\gamma n \rightarrow n\phi$  reaction.

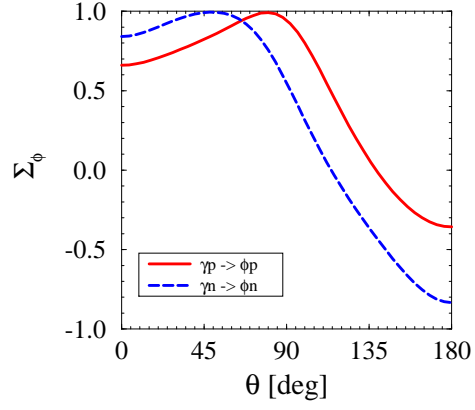


FIG. 5. The  $\phi$  decay asymmetry  $\Sigma_\phi$ , defined in Eq.(13), as function of  $\theta$  at  $E_\gamma=2$  GeV.

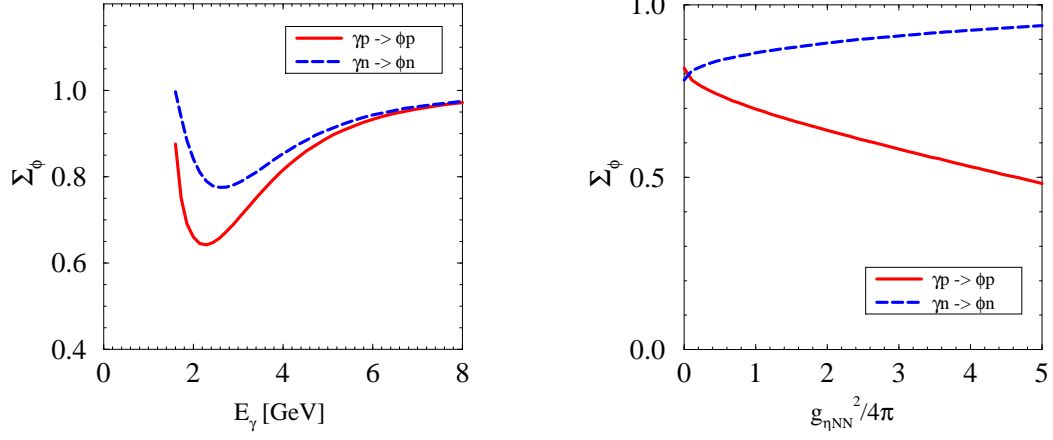


FIG. 6. The  $\phi$  decay asymmetry  $\Sigma_\phi$ , defined in Eq.(13), at  $\theta = 0$  as a function of the photon energy (left panel) and as a function of the  $\eta NN$  coupling constant (right panel).